Continental Shelf Research 77 (2014) 118–131

Contents lists available at ScienceDirect

Continental Shelf Research

journal homepage: www.elsevier.com/locate/csr

Research papers

# Oceanographic conditions in the Gulf of Mexico in July 2010, during the Deepwater Horizon oil spill

R.H. Smith [a,*], E.M. Johns [a], G.J. Goni [a], J. Trinanes [a,b], R. Lumpkin [a], A.M. Wood [a,1], C.R. Kelble [a], S.R. Cummings [a,2], J.T. Lamkin [c], S. Privoznik [c,d]

[a] Atlantic Oceanographic and Meteorological Laboratory, National Oceanic and Atmospheric Administration, 4301 Rickenbacker Causeway, Miami, FL 33149, USA
[b] Laboratory of Systems, Technological Research Institute, University of Santiago de Compostela, Campus Universitario Sur, Santiago de Compostela 15782, Spain
[c] Southeast Fisheries Science Center, National Marine Fisheries Service, National Oceanic and Atmospheric Administration, 75 Virginia Beach Drive, Miami, FL 33149, USA
[d] Cooperative Institute for Marine and Atmospheric Studies, Rosenstiel School of Marine and Atmospheric Science, University of Miami, 4600 Rickenbacker Causeway, Miami, FL 33149, USA

ARTICLE INFO

*Article history:*
Received 8 March 2013
Received in revised form
2 December 2013
Accepted 20 December 2013
Available online 28 December 2013

*Keywords:*
Deepwater Horizon oil spill
Gulf of Mexico oceanography
Loop Current
Eddy Franklin
Oil entrainment and transport
Subsurface oil plume

ABSTRACT

Circulation in the Gulf of Mexico (GOM) is dominated by mesoscale features that include the Loop Current (LC), Loop Current Rings (LCRs), and smaller frontal eddies. During May–June 2010, while oil was still flowing from the Macondo well following the Deepwater Horizon (DWH) platform explosion on April 20, 2010, drifter trajectories, satellite observations, and numerical simulations indicated a potential for direct connectivity between the northern Gulf and the Florida Straits via the LC system. This pathway could have potentially entrained particles, including northern GOM contaminants related to the oil spill, carrying them directly towards the coastal ecosystems of south Florida and northern Cuba. To assess this connectivity, and to evaluate the potential oil impacts on economically important GOM fisheries, an interdisciplinary shipboard survey was conducted in the eastern Gulf during July 2010. Analysis of the resulting hydrographic data confirmed that: (1) by July 2010 a large LCR had become separated from the main LC by a cyclonic eddy resulting in the loss of a direct transport mechanism from the northern GOM to the Florida Straits, leaving only indirect pathways available to potential contaminants; and (2) with the exception of four hydrographic stations occupied within 84 km of the wellhead, no evidence of oil was found during the survey on the surface or within the water column. These results corroborated analysis of satellite altimetry observations of the GOM surface circulation and verified official surface oil coverage forecasts where they intersected with the survey track. This cruise sampled the LC, LCR, and frontal eddies to a depth of 2000 m, with the results suggesting that any oil entrained by circulation features in prior months had either been weathered, consumed by bacteria, dispersed to undetectable levels, or was only present in unsurveyed areas. The assembled subsurface measurements represent one of only a few data sets collected across the dominant GOM mesoscale circulation features at a time when there was great concern about the potential long-range spreading of DWH related contaminants. Direct observations such as these are critical for the assessment of particle trajectory and circulation models utilized during the spill, and for the improvement of future numerical forecast products.

Published by Elsevier Ltd.

## 1. Introduction

Following the explosion and sinking of the Deepwater Horizon (DWH) drilling rig at the Macondo MC252 well on April 20, 2010, the northern Gulf of Mexico (GOM) was subjected to the largest offshore crude oil spill ever recorded in the western hemisphere (Adcroft et al., 2010; Camilli et al., 2010). Oil flowed continuously from the damaged wellhead for 87 days until it was capped on July 15, 2010 (Wells, 2010). During this time, 1100 miles of the northern Gulf coast were contaminated from the discharge (National Oceanic and Atmospheric Administration, 2012). Multiple ecosystems including marshes, mangroves, mudflats, and beaches were negatively impacted, requiring an unprecedented response effort. As of 2013, the recovery of these natural areas is an ongoing concern (Ramseur and Hagerty, 2013).

Unlike the majority of previous oil spills in the GOM, which occurred within 12 NM of the coastline (Kaiser and Pulsipher, 2007), the Macondo spill occurred ~41 NM from shore in deep water (1500 m) in the open ocean, in a region affected by strong surface and subsurface currents. The ocean environment had the

* Corresponding author. Tel.: +1 305 361 4328; fax: +1 305 361 4392.
*E-mail address:* ryan.smith@noaa.gov (R.H. Smith).
[1] Current address and affiliation: Department of Biology, University of Oregon, 77 Klamath Hall, 1210 University of Oregon, Eugene, OR 97403, USA
[2] (ret.).

0278-4343/$ - see front matter Published by Elsevier Ltd.
http://dx.doi.org/10.1016/j.csr.2013.12.009

potential to transport oil and dispersants to remote areas beyond the immediate spill site. This fact, which contributed to the extensive oiling along the northern Gulf coast, led to additional concerns regarding the possible southeastward spreading of oil towards Florida and beyond, aided by GOM mesoscale circulation features.

The dominant circulation features of the GOM include the Loop Current (LC), the Loop Current Rings (LCRs) which it sheds, and the numerous cyclonic eddies that tend to form along the LC and LCR frontal boundaries (Sturges and Leben, 2000; Zavala-Hidalgo et al., 2003; Schmitz et al., 2005). The LC is a component of the North Atlantic western boundary current system linking the Caribbean and Yucatan Currents to the Florida Current in the Florida Straits. The LC varies from a *young* configuration, where it flows nearly directly from the Yucatan Channel into the Florida Straits, to a *mature* configuration, in which it extends far into the northern GOM before retroflecting back toward the Florida Straits (e.g. Hetland et al., 1999).

When the LC is in an extended northward state, it tends to form and ultimately shed an anticyclonic (clockwise circulation) eddy, or LCR. LCRs are typically 200–300 km in diameter and their characteristic circulation may reach depths of up to ~1000 m. They possess swirl speeds of ~180–200 cm $s^{-1}$, move westward at ~2–5 km $day^{-1}$ (Oey et al., 2005), and have an average radial transport of ~29 Sverdrups (Sv; 1 Sv $\equiv 10^6$ $m^3$ $s^{-1}$) (Elliot, 1982). The LCR shedding process occurs at a frequency that can range from 3 to 21 months, and historical shedding activity has been shown to peak at 6, 9, and 11 months, with an average shedding frequency of 9.5 months (Sturges and Leben, 2000). After separating from the LC, LCRs may exist in the GOM for several months to one year (Oey et al., 2005).

Cyclonic (counter-clockwise circulation) frontal eddies are also often found along the edges of the LC and LCRs, and have been observed to play an important role in the LCR shedding process (Nowlin and McLellan, 1967; Zavala-Hidalgo et al., 2003; Schmitz et al., 2005). They can have swirl velocities $> 100$ cm $s^{-1}$ (Vukovich and Maul, 1985), are typically 50–150 km in diameter, and can extend to 1000 m depth (Oey et al., 2005).

When the LC is elongated into the northern GOM it is capable of transporting northern Gulf contaminants and Mississippi River discharge to remote downstream locations. In this configuration, the possibility for entrainment and direct delivery of northern Gulf waters to the Florida Straits and adjacent coastal ecosystems, such as the Florida Keys, is well documented and can occur in as little as two to three weeks (Ortner et al., 1995; Hu et al., 2005).

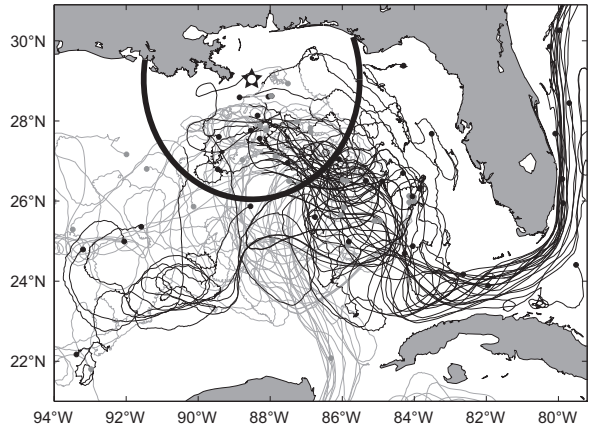


**Fig. 1.** Trajectories of all 48 NOAA GDP surface drifters, from January 1999 through November 2010, which passed within 3 degrees (black circle) of the DWH MC252 wellhead location (star). Satellite-tracked drifting buoys were drogued at a depth of 15 m to reduce downwind slippage and track the surface mixed layer (Niiler et al., 1995); drogue detection was conducted as described in Lumpkin et al. (2013). Trajectories prior to the point of closest approach are shown in gray (gray dot indicates deployment location). Trajectories after the point of closest approach are shown in black (black dot indicates location of final measurement).

Physical linkages between these regions are evident in the historical trajectories of all 48 Global Drifter Program (GDP) surface drifters that have traveled within 3 degrees of the MC252 wellhead location between January 1999 and November 2010 (Fig. 1). Consistent with previous GOM drifter studies (Yang et al., 1999; Olascoaga et al., 2006), these drifters indicated a stronger tendency to enter the Florida Straits, and ultimately the Atlantic basin, than to enter the southwest Florida Shelf, a region closer to the northern Gulf.

In the aftermath of the explosion and sinking of the DWH rig, the progression of the spill emanating from the damaged MC252 well was monitored remotely from satellites and aircraft, and directly via shipboard measurements, air-deployed expendable ocean profilers, and gliders (Streett, 2011; Lubchenco et al., 2012). These observations were augmented with outputs from several numerical models employed to simulate the GOM circulation at the surface and subsurface (Camilli et al., 2010; Hazen et al., 2010; MacFadyen et al., 2011). The scientific community involved in these monitoring and modeling efforts included researchers from government agencies, academia, and private industry.

In late April 2010, satellite altimetry observations indicated that the circulation in the GOM was dominated by a mature LC, which extended into the northern Gulf to ~27.5°N (Fig. 2a), and which had not shed a ring since July 2009 (Goni et al., submitted for publication). Though much of the initial movement of the spilled surface oil was shoreward towards the northern Gulf coast (late April / early May), some early numerical model results used to evaluate the potential spreading of surface oil from the spill supported the direct LC entrainment/transport scenario previously described (Lubchenco et al., 2012). In combination with the northerly location of the LC, these preliminary findings prompted response agencies and scientific institutions to pursue additional observational and modeling efforts over the broader eastern GOM in the event that the LC began to deliver DWH-related contaminants to remote downstream locations (Wood, 2010; Shay et al., 2011; Wade et al., 2011; Liu et al., 2011a,b).

Beginning in May 2010, airborne ocean surveys were conducted across the LC providing upper ocean temperature, salinity, and current velocity profiles (via 472 expendable ocean profilers; Shay et al., 2011). These data were assimilated into GOM Hybrid Coordinate Ocean Model (HYCOM) modeling efforts, ultimately reducing model biases by 50% and lowering model RMS errors by 30% (Shay et al., 2011). Also in May, satellite-tracked drifters began being deployed in the LC and across the eastern GOM (Liu et al., 2011a) to provide in situ observations of ocean currents. As the month progressed, surface current estimates derived from satellite altimetry indicated that a cyclonic circulation situated between the wellhead and the northern front of the LC began to entrain surface oil, drawing it farther offshore. Concurrently, the LC remained extended into the northern Gulf (eventually reaching a latitude of ~28.0°N between 85.0 and 88.0°W longitude). As a result, a filament of surface oil extended towards the southeast, aided by these two features (Fig. 2b). Tar balls sourced to MC252, possibly originating from this filament, were collected on June 8, 2010 as far south and east as 26°45.85′N, 86°03.65′W during one of the first research cruises to survey the LC region (Wood, 2010).

Satellite-derived fields of geostrophic surface currents and sea surface temperature (SST) documented the initial separation of a large anticyclonic LCR (named “Eddy Franklin”, hereafter EF) from the LC around May 16, and the subsequent interaction of these features with one another, including reattachment of the outer edge of EF on approximately June 15 (Fig. 2c). While EF separation may have inhibited direct connectivity between northern Gulf

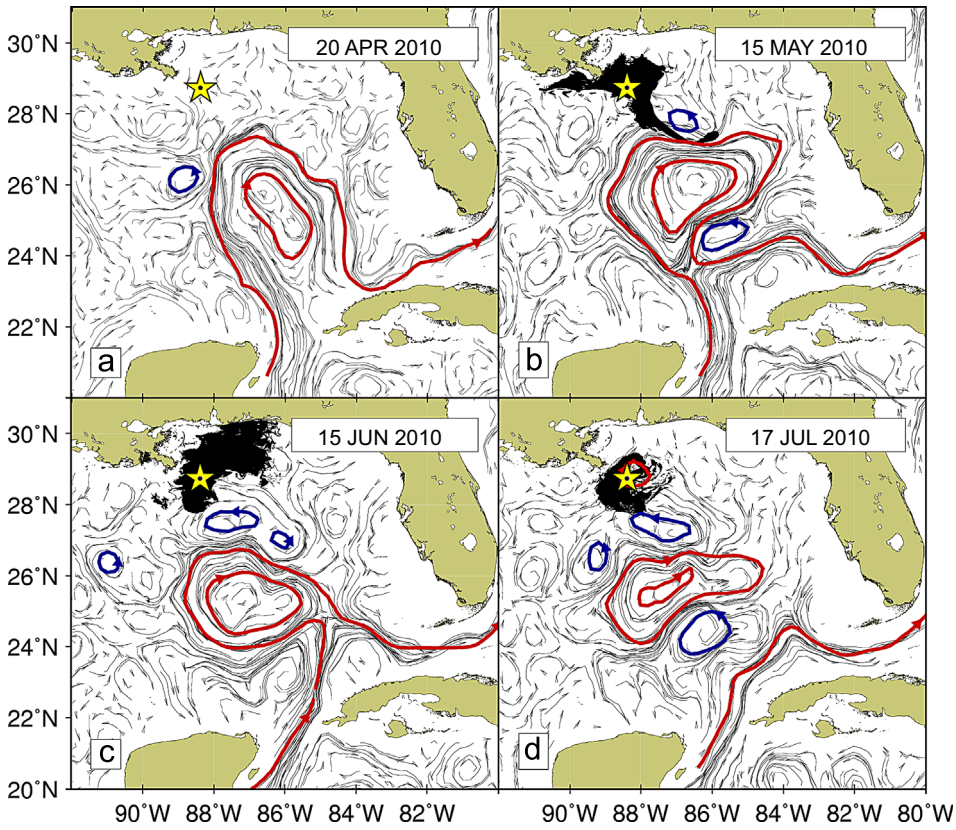


**Fig. 2.** Altimetry-derived surface velocity fields (gray vectors) are shown for selected dates: 20 April, 15 May, 15 June, and 17 July 2010 (panels (a)–(d) respectively). The major cyclonic (blue lines) and anticyclonic (red lines) mesoscale circulation features are indicated. Estimates of surface oil coverage for the same period (from NOAA/NESDIS) are shown in black (not available for 20 April). The location of the MC252 wellhead is marked with a yellow star.

regions and the Florida Straits, water particle trajectories obtained from numerical models using model and satellite-derived ocean current fields indicated that particles could still travel from the oil spill site into the southern GOM, albeit by a less direct route (Adcroft et al., 2010; Liu et al., 2011b). EF remained narrowly attached throughout the second half of June 2010. By the end of that month, the cyclonic features located on either side of the EF/LC region of attachment had served to zonally elongate the connection between the reattached EF and the LC. This resulted in a westward translation of EF and what appeared to be a second separation around June 28, 2010.

To further examine these connectivity issues and address the scarcity of in situ observations throughout the GOM, the National Oceanic and Atmospheric Administration (NOAA) Atlantic Oceanographic and Meteorological Laboratory (AOML) and the National Marine Fisheries Service (NMFS) Southeast Fisheries Science Center (SEFSC) jointly collected interdisciplinary oceanographic observations across the eastern GOM, utilizing the NOAA Ship *Nancy Foster*, between June 30 and July 18, 2010. The primary objectives of this shipboard survey were to: (a) Assess the physical connectivity (both surface and subsurface) between the complex eddy field formed by the LC, EF, and the other frontal eddies which developed over May and June; (b) document and sample any petroleum contaminants observed on the surface or at depth across the region; (c) provide in situ hydrographic data for the validation and initialization of numerical models employed during the spill; and (d) determine the potential impacts of any petroleum contaminants on pelagic fish larvae recently spawned in the eastern GOM. This article focuses on the results associated with the first two project objectives.

It is not our intent to provide a detailed review of, or new insight into, GOM circulation dynamics; this subject has been thoroughly examined in the literature. Rather, this work seeks to describe the surface and subsurface oceanographic conditions observed over a region of the Gulf which at the time of the DWH oil spill remained largely unsampled. Additionally, relevant findings from observations made within close proximity to the wellhead (in support of the larger coordinated spill site monitoring effort) will be presented. In Section 2, we describe our data collection and analysis techniques. This is followed by a discussion of our findings in context with other scientific work conducted as part of the response effort (Section 3). Finally, conclusions about the research are drawn in Section 4.

## 2. Observations and methods

### 2.1. Shipboard measurements

During the 19-day survey (June 30 to July 18, 2010), sampling was based upon the position of dominant GOM mesoscale circulation features such as the LC, EF, and frontal eddies. These feature locations were determined from the daily analysis of in situ data collected during the cruise, and remotely-sensed products such as altimetry-derived fields of geostrophic surface currents. Over this period, 73 stations were occupied and sampled with lowered/towed equipment while completing 15 hydrographic transects in the eastern GOM (total section coverage: ~3000 km). A complete accounting of survey operations may be found in Smith et al. (2010). Shipboard observations, samples, and methods relevant to this article are described below.

#### 2.1.1. Oceanographic instrumentation and analysis

Shipboard sampling was performed using an interdisciplinary suite of instruments. Conductivity–temperature–depth (CTD) casts were conducted from the surface to 2000 m, utilizing a Sea-Bird

Electronics (SBE) 9*plus* CTD, configured with dual temperature (SBE 3), conductivity (SBE 4), and oxygen sensors (SBE 43), chlorophyll *a* (chl_a) and colored dissolved organic matter (CDOM) fluorometers (both WET Labs ECO FL), and a 24-Niskin bottle water sampler. Two (upward and downward-looking) internally-logging, Teledyne RD Instruments 300 kHz lowered acoustic Doppler current profilers (LADCP) were also attached to the CTD frame. Continuous underway measurements of sea surface temperature, salinity, chl_a, and CDOM were collected using the onboard flow-through seawater system, which was equipped with an SBE 21 thermosalinograph (TSG) and Seapoint chl_a and ultraviolet fluorometers. Upper ocean current profiles (to ~250 m depth) were continuously recorded using a hull-mounted Teledyne RD Instruments 150 kHz shipboard acoustic Doppler current profiler (SADCP).

Discrete profiles of potential temperature ($\theta$) and salinity ($S$) collected during the CTD casts were classified objectively according to their similarity to three prototypical $\theta$–$S$ signatures recorded during the survey in different water mass and circulation features. The selected profile prototypes were designated as LC Water (LCW), measured in the LC south of the west Florida shelf (24°17.6′N, 83°57.0′W); Gulf Common Water (GCW), measured in the center of the cyclonic eddy situated between the LC and EF in early July (24°47.0′N, 85°42.1′W); and EF Core Water (EFCW) measured in the center of EF (25°29.7′N, 87°30.9′W). These prototypes (Fig. 3) were selected based upon historical GOM circulation and water mass literature (c.f. Nowlin and McLellan, 1967; Nowlin, 1972; Schroeder et al., 1974; Paluszkiewicz et al., 1983; Jochens and DiMarco, 2008). CTD data, originally binned by pressure at 1 decibar intervals, were linearly interpolated to a standard potential density ($\sigma_\theta$) interval of 0.05 kg m$^{-3}$ to allow for the comparison of salinities between stations on identical density surfaces ($\sigma_\theta \equiv \rho_\theta - 1000$ kg m$^{-3}$). For each cast, the interpolated data located on and between the isopycnal surfaces $\sigma_\theta$=24.0 kg m$^{-3}$ and $\sigma_\theta$=26.0 kg m$^{-3}$ were selected for comparison. This density range excludes the majority of the highly variable surface waters while capturing the characteristic differences of the prototypes selected (Fig. 3). At densities greater than $\sigma_\theta \approx 26.5$ kg m$^{-3}$, $\theta$–$S$ relationships of the GOM CTD profiles become relatively indistinct from one another, due to their common origin via the LC system.

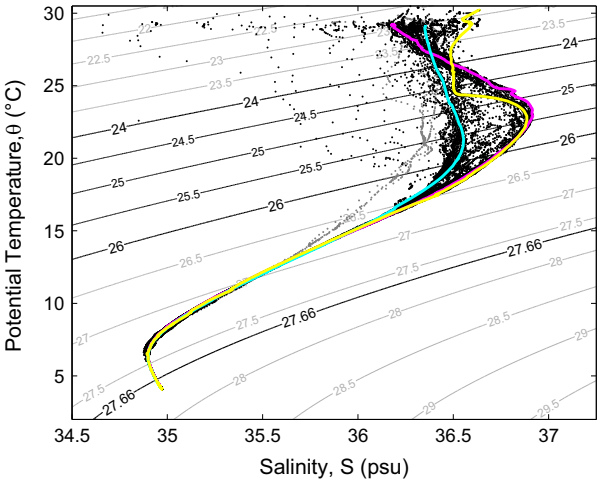


**Fig. 3.** The relationship of potential temperature ($\theta$) to salinity ($S$) for CTD profiles collected during the survey is shown over contours of constant $\sigma_\theta$ (in kg m$^{-3}$). Three prototypical profiles, selected from stations conducted during the July survey, have been highlighted: GCW (blue), LCW (magenta), and EFCW (yellow). Profile data collected between $24.0 \le \sigma_\theta \le 26.0$ were used in the cast classification. Data points shown in dark gray correspond to five casts conducted along the northern end of the Key West–Havana section (Section A). The distinct $\theta$–$S$ relationship of these casts is associated with the entrainment of water from the shallow southwest Florida shelf (north of the section) by a decaying frontal eddy situated across the northern end of the transect.

Each selected salinity data point was first compared to the GCW and LCW prototype values at the same density. The salinity data point was then classified as either GCW or LCW depending on which of the two corresponding prototype salinities was closer. Salinities initially binned as GCW were subsequently further examined. If an individual salinity was saltier than the GCW prototype by at least 0.05 practical salinity units (psu), or if it was fresher than the GCW prototype salinity by 0.05–0.10 psu, it was reclassified as *mixed/interleaved*. If the salinity was fresher than the GCW prototype salinity by even more than 0.10 psu, it was reclassified as Coastal Shelf Water (CSW). Salinities binned initially as LCW were also subsequently re-examined. Those that were found to be fresher than the LCW prototype salinity on the same density surface by 0.05 psu or more were reclassified as mixed/interleaved.

Following the individual density interval salinity analysis, each $\theta$–$S$ profile was examined as a whole (over the range $24.0 \le \sigma_\theta \le 26.0$ kg m$^{-3}$). The overall profile was classified by the most prevalent water type (GCW, LCW, CSW, or mixed/interleaved). If none of the water types totaled more than 2/3 of the identifiers for the entire density range, the profile was labeled as mixed/interleaved. As EFCW was essentially a specific type of mixed $\theta$–$S$ signature, with a characteristic subtropical underwater salinity maximum (owing to its recent LCW origin) topped with a unique layer of constant salinity, profiles classified as mixed/interleaved were tested for their likeness to the EFCW prototype. If the absolute mean difference (computed from all absolute salinity differences, at each 0.05 kg m$^{-3}$ density interval) between the salinity profile and the EFCW prototype was $\le$0.02 psu, the profile was reclassified as EFCW. In some cases, a CTD cast may not have been deep enough to record any water denser than $\sigma_\theta$=24.0 kg m$^{-3}$; these stations remained unclassified.

SADCP and LADCP velocity measurements were used to examine the surface and subsurface structure of the various circulation features observed across the survey domain to a depth of 2000 m. In most cases, these features exhibited a surface expression similar to that observed in velocity fields derived from satellite altimetry, and both in situ and remotely-sensed velocity data were used while underway to guide the survey. The SADCP data were processed with the Common Ocean Data Access System (CODAS) developed at the University of Hawaii (http://currents.soest.hawaii.edu/docs/adcp_doc/codas_doc/), and LADCP data were processed using the GEOMAR Visbeck software v10.8 (Visbeck, 2002). Although not central to this study, volume transports across the major sections/features surveyed were also calculated using the merged in situ velocity data set (SADCP and LADCP). These transports, and the methods employed to calculate them, are detailed further in the Appendix.

### 2.1.2. Oil/Hydrocarbon sampling

Methods for observing surface oil and tar balls over the survey region included visual observations of the sea surface during daylight hours, net tows, and the flow-through Seapoint ultraviolet fluorometer (SUVF). Visual observations were conducted from the bridge, flying bridge, or bridge wing of the ship by watchstanders or by a dedicated observer.

The nets employed for icthyoplankton sampling were simultaneously used to sample for tar balls and weathered oil. Surface net tows, including Spanish bongo (505 μm mesh), Spanish neuston (505 μm mesh), and standard neuston (947 μm mesh) nets, were towed for 10 min at an average speed of 1 m s$^{-1}$. Though considered a surface tow, Spanish bongo and neuston tows were cycled between the surface and a depth of 10 m ten times during

each tow. The profiling 1 $m^2$ MOCNESS (Multiple Opening and Closing Net Environmental Sampling System) was equipped with 5 nets (505 μm mesh), and towed at a speed of 1 m $s^{-1}$. The system was typically lowered at 7–10 m $min^{-1}$ and hauled in at 5–7 m $min^{-1}$. It sampled depths of 0–100 m (downcast net), 100–75 m, 75–50 m, 50–25 m, and 25–0 m. Following each tow, nets and net frames were visually examined for the presence of tar balls. The standard neuston tows should have permitted capture of tar balls and semi-solid masses of weathered oil $>1$ mm in diameter; all other tows should have captured even smaller particles ($>0.5$ mm).

The search for oil and hydrocarbon contaminants within the water column relied upon two types of measurements: dissolved oxygen ($O_2$) and fluorescence. Data from the CTD dual SBE 43 $O_2$ sensors were used as an indirect proxy for subsurface oil, as anomalous $O_2$ minima could indicate either potential microbial degradation of oil or the presence of methane (Kessler et al., 2011; Joye et al., 2011). Additionally, the CTD WET Labs ECO FL CDOM fluorometer was employed to detect the fluorescence of oil in subsurface layers.

Although CDOM fluorometers were commonly used in the search for hydrocarbons during the spill response (Diercks et al., 2010; Ryan et al., 2011), the effectiveness of these repurposed instruments was limited by their design parameters. Crude oil is a combination of hydrocarbon components that, as a mixture, typically fluoresce strongly when excited in the ultraviolet spectrum at wavelengths around 300 nm, and may emit broadly from 300 nm to beyond 500 nm, but generally show peak emission in the blue region of the spectrum (Green et al., 1983; Bugden et al., 2008). When trying to measure hydrocarbons from a specific source by optical means, ideally a fluorometer would be tuned to the precise excitation (EX) wavelength which yields a maximum emission (EM) wavelength for the source oil which will have specific, unique fluorescent properties (Bugden et al., 2008). Following standardization with source material, such an instrument could then be calibrated to report a first order estimate of source specific oil concentration. However, this scenario assumes the optical properties of the target oil to be stable. Empirically this is not the case, as dispersal and/or the natural weathering of crude oil will change its fluorometric response (Henry et al., 1999). Given that such an instrument was not available for deployment, fixed wavelength ultraviolet fluorometers with EX/EM ranges designed to measure CDOM, but which fall within the crude oil EX/EM spectrum, were deployed for this study (WET Labs ECO: 350 nm EX / 430 nm EM; Seapoint: 370 nm EX / 440 nm EM). A similar repurposed WET Labs ECO fluorometer identified a CDOM fluorescence peak earlier in the spill near the MC252 wellhead at depths $>1000$ m which was confirmed to be due to the presence of hydrocarbons (Diercks et al., 2010). Additionally, WET Labs provided preliminary data indicating that the ECO CDOM fluorometer was sensitive to the presence of hydrocarbons. Thus, the use of these fluorometers as preliminary indicators for the possible presence of hydrocarbons and to target sample collection was reasonable.

### 2.2. Satellite observations

During the DWH oil spill, ocean conditions and surface oil coverage were continuously monitored utilizing data from multiple satellite sources. These data complemented the in situ observations and proved to be critical assets for spill response decision-making (Lubchenco et al., 2012). Satellite measurements used in our analysis included sea surface height (SSH) fields derived from satellite altimetry, and a merged synthetic aperture radar (SAR) / visible and near-infrared (VNIR) imagery product (produced by NOAA/NESDIS, Satellite Analysis Branch).

Each daily composite SSH field was constructed using 10 days of 7 km resolution, along-track AVISO altimetry data and a global mean dynamic topography (CNES-CLS09, as described in Rio et al., 2011). The repeat cycle of the altimeters contributing to the AVISO product ranged from 10 days (Jason-1 and Jason-2) to 35 days (Envisat). Horizontal gradients in the SSH fields were used to estimate daily surface geostrophic currents, and from their spatial gradients, to determine the locations of the fronts associated with anticyclonic and cyclonic features. These maps provided basin-wide coverage of surface circulation dynamics in the GOM.

## 3. Results and discussion

### 3.1. GOM mesoscale circulation features in July 2010

The collected hydrographic data provided important in situ information about the surface and subsurface currents and water properties associated with the LC, EF, cyclonic eddies, and the surrounding coastal waters of the GOM. Variations in the horizontal velocity structure and in the subsurface $\theta$–$S$ relationships helped to assess the level of physical connectivity across the survey region and to determine the degree of mixing and interleaving between the major circulation features. When the spatial distribution of the $\theta$–$S$ signature groupings (described in Section 2) is overlaid upon SADCP derived current vectors, the location of the various signature types in relation to the surface velocity associated with each circulation feature becomes evident (Fig. 4).

In early July 2010, in situ surface velocity measurements confirmed altimetry estimates which revealed that the northern edge of the LC was impinging upon the southwest Florida shelf at ~24.75°N, 84.0°W, near the mesophotic reef known as Pulley Ridge (Fig. 4), before turning southeast and entering the Florida Straits (Sections B–E in Fig. 4, and Fig. 5a and 5b). Evidence of mixing and entrainment of both CSW and GCW with LCW is evident from $\theta$–$S$ profiles collected along Section E in this vicinity. Inshore of this location, between Pulley Ridge and the Dry Tortugas (Fig. 4), a strong southward flow associated with this LC retroflection was observed across the southwest Florida shelf. This flow entrained CSW, drawing it southward into the Florida Straits. This entrainment is also evident farther east at Section A, where a decaying cyclonic frontal eddy situated across the northern end of the section possessed a unique $\theta$–$S$ signature attributable to the CSW (dark gray profiles shown in Fig. 3).

A cyclonic eddy, located at ~24.8°N, 85.5°W on July 9, with a radius of ~120 km and a maximum recorded swirl velocity of 171 cm $s^{-1}$, was observed in the altimetry and hydrographic data over multiple transects of the cruise track (Sections E–J in Fig. 4 and Fig. 5a–d). This circulation feature, which later translated westward, was partly responsible for the separation of EF from the LC. Though not evident in Section E (Fig. 5b), velocity sections for transects G and J (Fig. 5c and 5d) revealed a cyclonic circulation extending to a depth of at least 2000 m (the maximum depth of the CTD/LADCP casts). The presence of this deep cyclonic circulation (Fig. 6) is in general agreement with previous work on deep GOM circulation (DeHaan and Sturges, 2005). It is unclear if the observed velocities below 1000 m were directly related to the upper-ocean, surface-intensified circulation or to some other deep GOM circulation dynamic such as topographic Rossby wave propagation (TRW; Hamilton, 1990; Oey and Lee, 2002). The water column near the center of the measured circulation exhibited GCW $\theta$–$S$ profile characteristics. However, many stations revealed a mixed/interleaved water column with evidence of both GCW and LCW $\theta$–$S$ signatures, suggesting enhanced mixing along the frontal boundaries (Fig. 4).

The westernmost CTD/LADCP station along Section E, conducted on July 8, revealed an EFCW $\theta$–$S$ signature (yellow profile, Fig. 3) with a layer of constant salinity and decreasing temperature in the upper water column (to a depth of ~130 m) above the

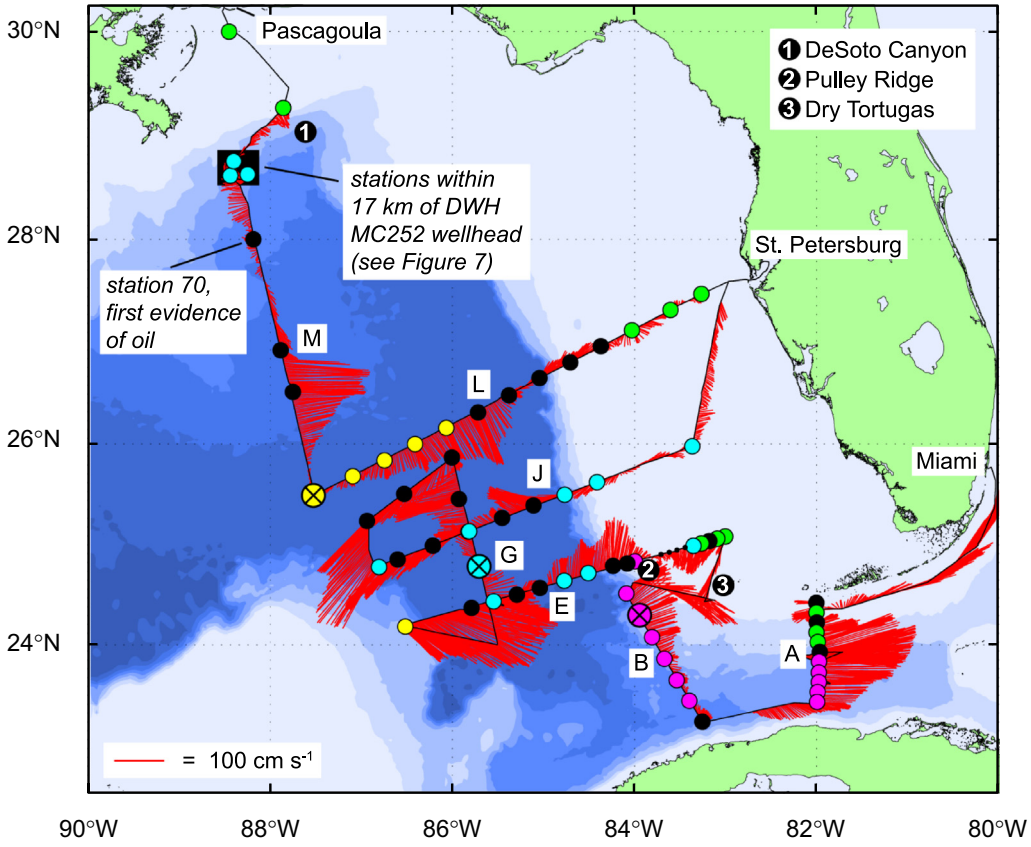


**Fig. 4.** In-situ surface current velocity from SADCP (red vectors) and CTD/LADCP station markers are shown above for the July 2010 survey. Marker colors indicate the station $\theta$–$S$ profile classification as either GCW (blue), LCW (magenta), EFCW (yellow), CSW (green), or mixed/interleaved (black). Stations lacking waters denser than $\sigma_\theta$=24.0 kg m$^{-3}$ are shown as small black dots. Prototype profile locations are indicated by an "$x$" and an enlarged marker. Letters identify selected sections along the cruise track. Sea floor elevations are contoured at 500 m intervals.

characteristic LC salinity maximum. This can occur when these waters are exposed to wind-driven mixing and the development of a deep mixed layer in winter months, followed by summertime heating and the restoration of a seasonal thermocline (Elliot, 1982). Prior to the separation of EF, waters recirculating within the center of the LC loop were subjected to such a scenario, as the LC had not previously shed a ring since July 2009. This profile (which was markedly different from those observed at previous stations) in conjunction with concurrent satellite and in situ velocity fields, confirmed that the survey had, for the first time, reached the anticyclonic EF circulation, located to the west of the large cyclonic frontal eddy. Additionally, continuous surface measurements collected along the ship track indicated that significantly higher sea surface salinities and lower chl_a and CDOM fluorescence were found in EFCW than LCW (not shown). This suggests that at the time of the survey the surface separation of EF from the LC was great enough to allow for distinct biogeochemical signatures to have developed, likely as a result of the long residence time within the center of EF which isolated the seawater from terrestrial sources of freshwater and nutrients.

Velocity Section E shows this station location to be ~40 km west of the strongest flows associated with EF and the adjacent cyclone (yellow marker in Fig. 5b). Further evidence of EFCW was not observed during subsequent transects G–J, conducted over the following four days (July 8–12, 2010). This supported altimetry fields and surface drifter trajectories (not shown) which documented further separation of EF from the LC, including a westward translation and zonal (east–west) elongation of EF from July 7 to July 17 (Fig. 2d).

Two radial transects (Sections L and M) were conducted across EF during the survey, revealing a surface-intensified flow (Figs. 4 and 5e–h). Section L confirmed an elongated EF radius of ~245 km. The maximum swirl velocity recorded along this section was found to be 107 cm s$^{-1}$ at a distance of ~175 km from the center of circulation. EFCW $\theta$–$S$ signatures were observed at all CTD/LADCP stations inside of this distance (Fig. 4). Beyond 185 km from the center, mixing and interleaving with GCW was evident in the $\theta$–$S$ profiles, indicating entrainment of surrounding waters along the EF circulation front. Section M, conducted from slightly south of the approximate center of the EF circulation to the western DeSoto Canyon and MC252 wellhead, revealed a smaller eddy radius of ~175 km and an associated swirl velocity maximum of 164 cm s$^{-1}$ (Fig. 4, and Fig. 5g and 5h). This maximum was located ~113 km from the center of EF. Although the CTD/LADCP stations were more widely spaced along Section M due to time constraints, continuous SADCP data collection allowed for the targeted positioning of stations on either side of the EF swirl velocity maximum. While the $\theta$–$S$ relationship of water sampled on the southern side of this maximum was ultimately classified as mixed/interleaved (Fig. 4), of the three $\theta$–$S$ prototypes, it most closely resembled EFCW. North of the maximum (~135 km from the center of circulation), CTD data revealed a mixed $\theta$–$S$ profile most closely resembling GCW. The limited LADCP profiles collected across Section M suggested that the circulation associated with EF extended to a depth of ~1120 m (Fig. 5h). Though a similar definitive cutoff was not evident in Section L (Fig. 5f), 1120 m swirl velocities along this section were $<$12 cm s$^{-1}$. Assuming a circular ring, the in situ velocity data suggest that

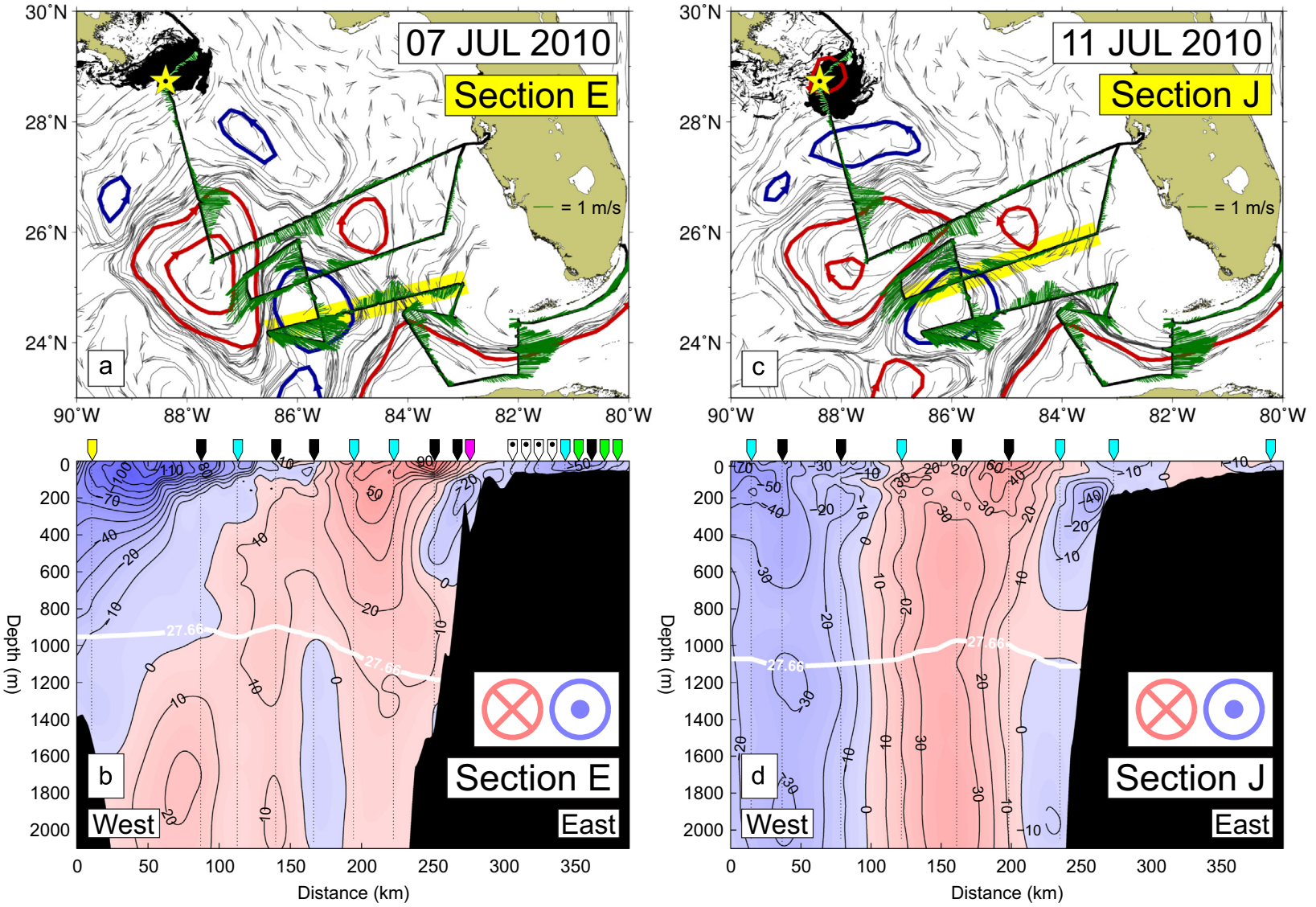


**Fig. 5a–d.** SADCP surface current vectors (green) are plotted with synoptic fields of altimetry-derived surface velocity (gray) for the highlighted Sections E and J. The major cyclonic (blue lines) and anticyclonic (red lines) mesoscale circulation features are indicated. The location of the MC252 wellhead is marked with a yellow star, and an estimate of surface oil coverage for the same period (from NOAA/NESDIS) is shown in black (panels a and c). Current velocity structure, normal to the section, produced from continuous SADCP data (Section E coverage to ~200 m, Section J coverage to ~250 m) and discrete LADCP data (dotted vertical lines; coverage to 2000 m) is also presented (panels b and d). Labeled velocity contours (black lines) are shown in cm $s^{-1}$. The single white density contour represents the 27.66 kg $m^{-3}$ isopycnal. θ-S profile classifications (from Fig. 4) are also shown for each CTD station along the section (colored pointers).

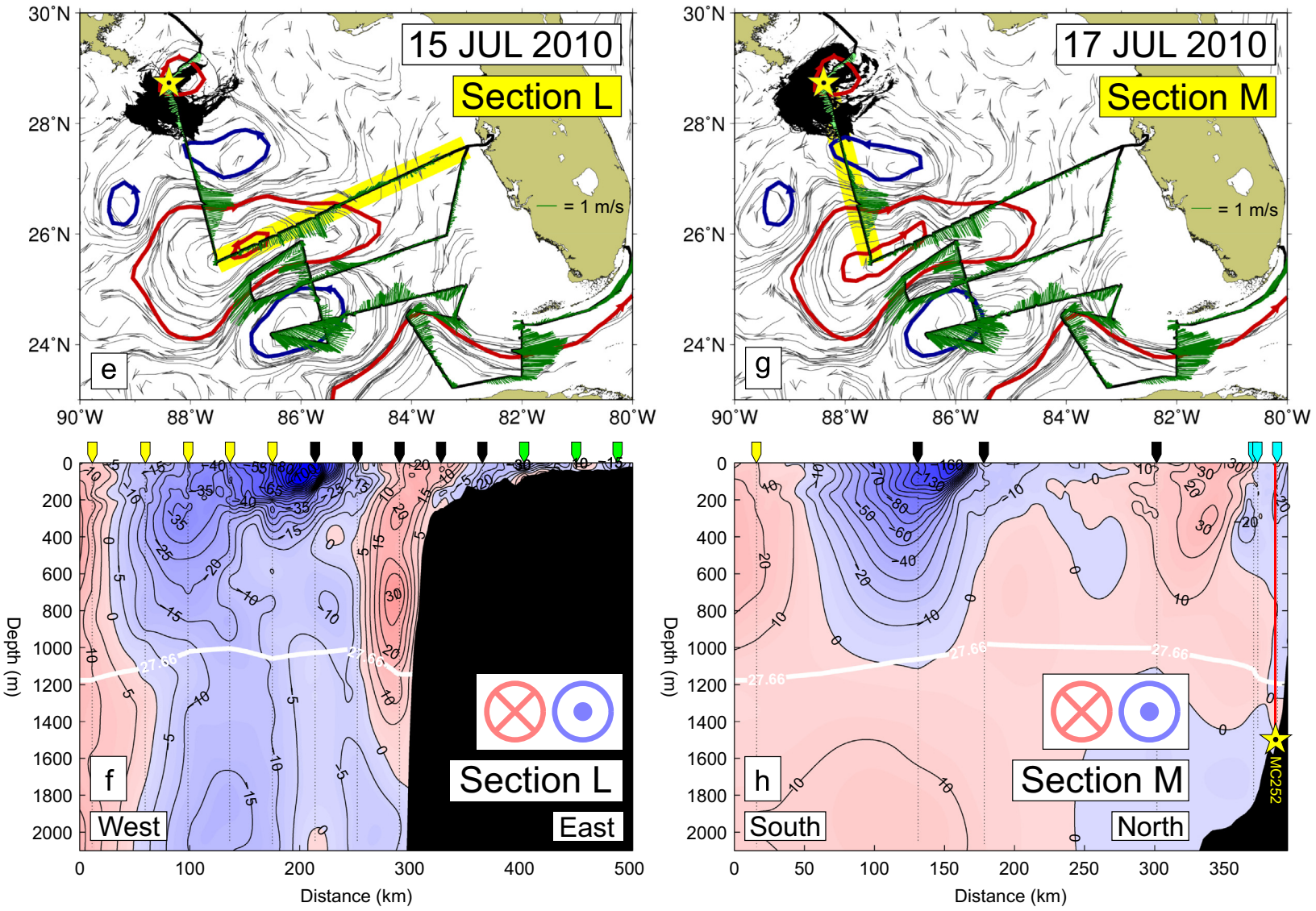


**Fig. 5e–h.** Same as Fig. 5a-d for Sections L and M (continuous SADCP coverage on Section L to a depth of ~250 m, on Section M to depths from ~250 to ~350 m).

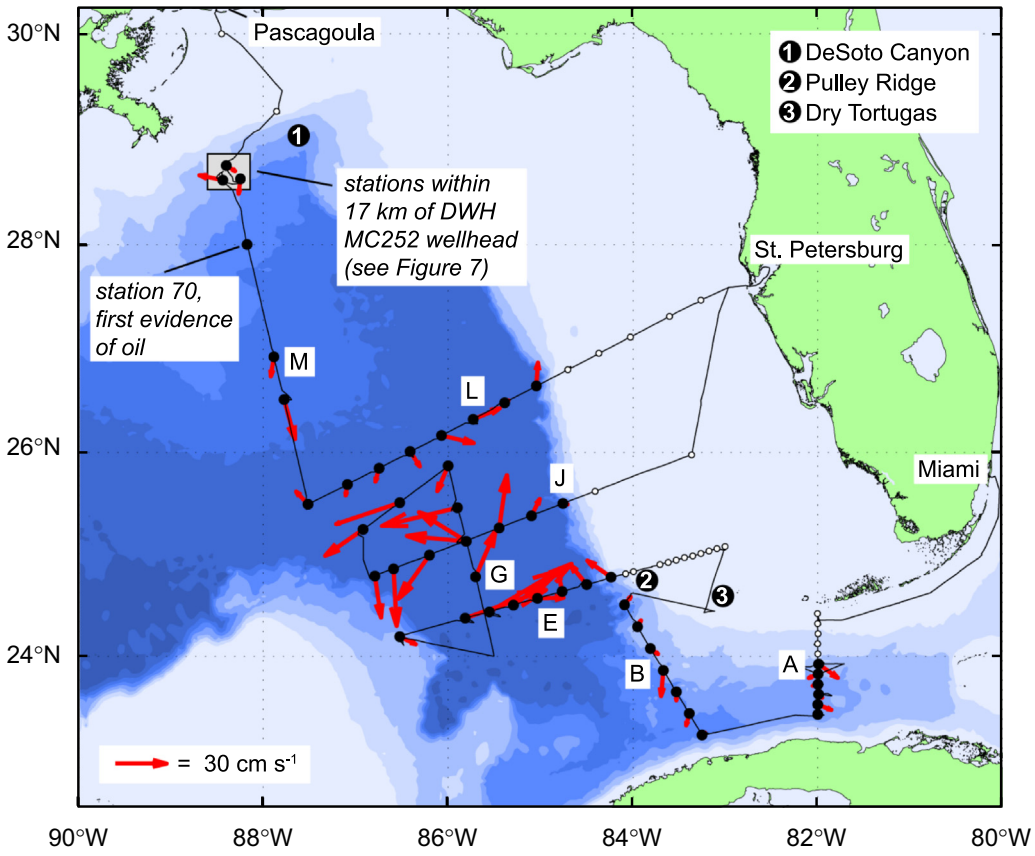


**Fig. 6.** LADCP current vectors representing the flow at 1100 m (the approximate depth of $\sigma_\theta = 27.66$ kg m$^{-3}$ over the region) are shown above for the July survey. Station locations are marked in black, except where water depths were shallower than 1100 m (shown in white). Sea floor elevations are contoured at 500 m intervals.

entrained particle revolution about the center of EF should take a minimum of 5 (Section M) to 12 (Section L) days. However, due to the irregular shape of EF, the rotational period may have been quite different than this estimate.

### 3.2. Surface and subsurface oil findings

Prior to Section M (Figs. 4 and 5a–f), no evidence of oil was observed visually on the sea surface, collected in nets, recorded in the continuous sea surface CDOM data set, or measured by the lowered CTD CDOM and $O_2$ sensors. Sections A–L included multiple regions of convergence and mixing along frontal zones where DWH contaminants, if present, might have been expected. This suggests that if any oil was present, it was at a concentration below our varying limits of detection (see Section 2.1.2). The lack of any strong oil signal attributable to the Macondo well over Sections A–L is in agreement with Wade et al. (2011) who report on 282 surface and subsurface samples tested for hydrocarbons, collected during a multi-leg research cruise conducted across the LC region (between 25°N and 27°N) at approximately the same time period as this survey (June 27–July 24, 2010).

Over the ~200 km distance between EF and the MC252 wellhead, both a cyclonic eddy south of the wellhead and a small anticyclonic eddy surrounding the wellhead were observed (Section M in Fig. 4, and Fig. 5g and 5h). In situ current velocity measurements in these features revealed a surface-intensified swirl velocity maximum of ~30 cm s$^{-1}$. Both eddies were also clearly visible in the altimetry-derived surface velocity fields for the period (Figs. 2d and 5g). Surface oil and tar balls were first visually observed 84 km south of the wellhead, within the cyclonic eddy, inside of official oil forecast boundaries[3] at station #70 (Figs. 4 and 6). The concentration of polycyclic aromatic hydrocarbons (PAH) measured[4] in surface samples collected at this station ranged between 49 and 132 ng L$^{-1}$. The SADCP/LADCP velocities (Fig. 5h), and the location of these findings on the northern side of the cyclonic circulation (Fig. 5g), suggest that any entrained contaminants would be carried westward (and then southward) prior to potential mixing along the northern EF front, thus lengthening the indirect pathway between the western DeSoto Canyon and the prominent circulation features south of 27°N.

On July 17, three CTD/LADCP stations were conducted at the northern terminus of Section M within 17 km of the MC252 wellhead (station #71, #72, and #73; Fig. 7). The location of these stations was coordinated with other survey and response vessels on site (Smith et al., 2010). Though intermittent surface sheens were spotted while sampling the area, no tar balls were observed while conducting these stations. However, at station #71, dark oily smudges were discovered on both the 0–100 m MOCNESS net and the standard neuston net (both of which sample surface water) following each tow. PAH concentrations in surface water samples collected at these three stations were less than 40 ng L$^{-1}$.

[3] Daily oil coverage forecasts were produced by the NOAA Office of Response and Restoration (ORR) and by NOAA/NESDIS/SAB. These products are available online at http://response.restoration.noaa.gov and http://www.ssd.noaa.gov/PS/MPS/deepwater.html, respectively.

[4] Hydrocarbon analysis of frozen seawater samples was performed using gas chromatography / mass spectrometry (GC/MS). Samples were processed by the Response and Chemical Assessment Team (RCAT) laboratory at Louisiana State University.

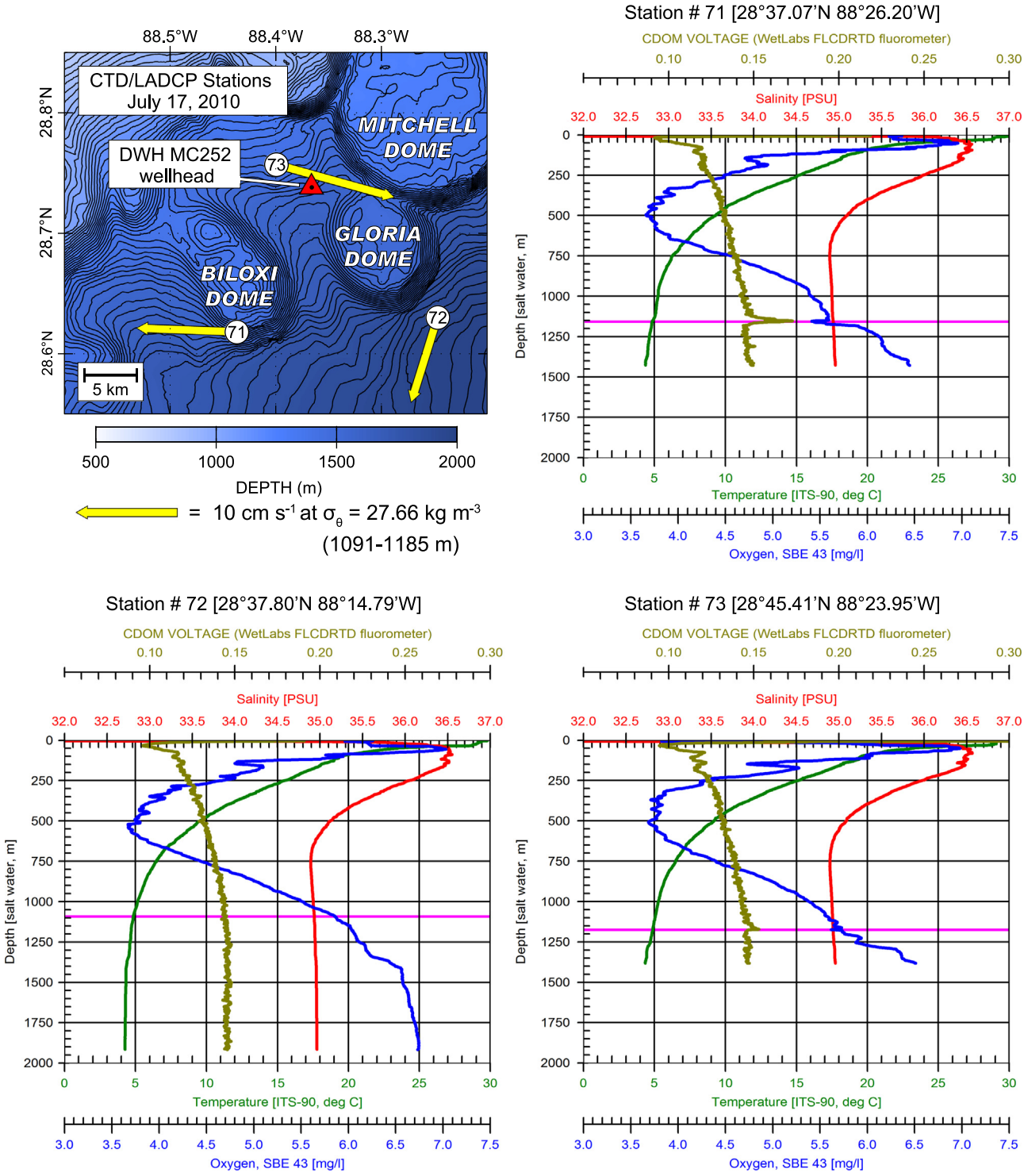


**Fig. 7.** CTD/LADCP hydrography conducted near the DWH MC252 wellhead on July 17, 2010. CTD profiles of temperature, salinity, $O_2$, and CDOM are shown for stations #71–#73. Indications of a potential subsurface hydrocarbon plume are visible in the CDOM and $O_2$ profiles at stations #71 and #73. The horizontal magenta line in each plot corresponds with a density layer of $\sigma_\theta$=27.66 kg m$^{-3}$ where, at station #71, the strongest signals observed in CDOM and $O_2$ were observed. LADCP velocity vectors are plotted for the density layer equivalent depth at each station. The flow at these depths (1091–1185 m) was approximately 10 cm s$^{-1}$ with variable directionality.

Evidence of a potential subsurface hydrocarbon plume concentrated around a density surface of $\sigma_\theta$=27.66 kg m$^{-3}$ was observed in CDOM and $O_2$ water column profiles collected at stations #71 and #73 (isopycnal indicated with white contours in Fig. 5, and horizontal magenta lines in Fig. 7). This corresponds to a depth range of 1091–1185 m over the three locations. The location and depth of this observation is similar to findings of other investigators who studied the spreading of subsurface oil during the spill (Camilli et al., 2010; Diercks et al., 2010; Hazen et al., 2010). Current velocity magnitudes at these depths for the three stations were observed to be ~10 cm s$^{-1}$ with variable directionality (Fig. 7).

The strongest subsurface anomalies in CDOM (an increase) and in $O_2$ (a decrease) were observed at station #71 at a depth of

1154 m, 15 km south–southwest of the wellhead (28°37.1′N, 86°26.2′W) (Fig. 7). PAH concentrations ranging from 335 to 410 ng $L^{-1}$ were measured in water samples collected from this station/depth. Additionally, fluorescence excitation emission matrix spectroscopy (EEMS) confirmed that these samples showed anomalous EEMS features, similar to samples collected by other researchers at approximately the same depth near the MC252 spill site (P. G. Coble, personal communication). PAH concentrations observed in deep samples collected from stations #72 and #73 were less than 35 ng $L^{-1}$.

CTD $O_2$ sensors generally recorded a more gradual signal decrease (compared to the corresponding CDOM voltage increase) in $O_2$ concentrations near the suspected feature, over a broader depth range (between 950 and 1400 m), resulting in a "scalloped" $O_2$ profile (Fig. 7). This may have resulted from microbial degradation of oil or accompanying methane within the water column, which can intensify $O_2$ depletion (Kessler et al., 2011; Joye et al., 2011). These observed decreases in $O_2$ were subsequently verified by photometric Winkler titrations performed onboard using water samples collected at depth.

LADCP current vectors corresponding to similar depths (~1100 m) farther south along sections L and M generally indicated southward flow (Fig. 6). If contaminants were present along these sections, at (or around) the 27.66 kg $m^{-3}$ isopycnal (Fig. 5f and 5h), they could have potentially been advected via the deepest extent of EF circulation, or possibly deeper circulation processes such as TRW. TRW are the predominant circulation influence in the GOM below 1000 m (Hamilton, 1990; Oey and Lee, 2002). While they are not directly correlated with coincident upper-layer LC, LCR, and frontal eddy activity, they are spawned via energy transfer from these features (Hamilton, 2009). However, regardless of the mechanism, there was no indication of a deep hydrocarbon plume evident in any of our CTD data collected prior to station #71. Additionally, flows between the wellhead and EF at this density surface were extremely weak. For example, the current velocity corresponding to the 27.66 kg $m^{-3}$ isopycnal at station #70 (where surface oil was first observed; Figs. 4 and 6), was found to be less than 5 cm $s^{-1}$ (towards the southwest).

## 4. Conclusions

A research cruise collected a suite of environmental observations across the eastern GOM in July 2010. The survey region encompassed the dominant mesoscale circulation features that could have potentially carried spill-related contaminants to remote downstream ecosystems. Prior to the cruise, this portion of the Gulf had remained largely unsampled by direct methods following the DWH explosion in April. During May and June, there was much speculation about the fate of oil-related contaminants across the broader GOM. Modeling efforts yielded multiple oil transport and particle trajectory scenarios and a limited number of samples collected south of the northern Gulf had actually been sourced to the MC252 well. However, prior to the July cruise, a comprehensive search for DWH-related contaminants, both at the surface and within the water column across these circulation features, had not been conducted. Even if a direct pathway had existed between the northern Gulf and remote downstream regions, the significance of such a scenario would have depended completely on the type, quantity, location, and degradation of any contaminants entrained.

We conclude, from our analysis of the in situ hydrographic measurements and velocity profiles obtained during this survey, that by July, a direct pathway capable of entraining and transporting northern GOM particles directly to the Florida Straits, with limited mixing en route, was no longer in place. In addition to confirming GOM altimetry observations of the surface circulation, these oceanographic data allowed for a unique characterization of the subsurface water mass and velocity structure associated with the complex eddy field present across the eastern GOM during July 2010. This analysis verified the separation of the large LCR, named Eddy Franklin, from the LC both at the surface and at depth, which subsequently partially acted as a physical barrier between the northern GOM and downstream ecosystems by retaining any material potentially entrained within its circulation away from coastal areas.

Second, results obtained from this survey found no evidence of surface oil south of 28°N along the cruise track. Surface oil was only observed near the end of the cruise, within 84 km south of the spill site and inside of the official oil forecast boundaries. Similarly, evidence of a subsurface hydrocarbon plume was only detected at a small number of stations within close proximity (15 km) to the MC252 wellhead. This result is consistent with other findings for the period, which suggested that most movement of the DWH subsurface oil plume appears to have been towards the southwest, flowing along a layer of neutral density at approximately 1100 m depth and paralleling nearshore bathymetric contours of the northern GOM (Camilli et al., 2010; Parsons and Cross, 2010), in an area unsampled by this survey. Uncontrolled output from the MC252 wellhead was finally arrested on July 15, 2010, three days prior to the conclusion of the research cruise. The lack of tar balls, surface sheens, or CDOM and $O_2$ profiles with signatures indicative of subsurface hydrocarbon plumes over the broad study domain, south of the official oil forecast boundaries, suggests that any oil that may have been carried to the southern GOM survey area prior to the July cruise had either been weathered, consumed by bacteria, dispersed to levels undetectable by methods employed during the cruise, or was only located in unsurveyed areas. Model results which incorporated oil degradation and dispersion (Adcroft et al., 2010) and evidence for shortened oil longevity in the water column due to microbial degradation (Hazen et al., 2010; Valentine et al., 2010; Joye et al., 2011) support the first three possibilities.

By August 2010, satellite altimetry indicated that the zonally-elongated EF had translated southward and once again reattached to the LC (Goni et al., submitted for publication). At that time, several GDP drifters which had been circulating within EF were abruptly ejected to the east and proceeded to move along the LC front, corroborating the altimetry result that at least a fraction of the eddy had reattached with the LC (not shown). However, with no strong circulation observed north of 27°N, no detectable oil en route prior to August, and no additional MC252 oil entering the Gulf following July 15, it is unlikely that any contaminants were available for entrainment into this more direct LC circulation pathway.

In situ observations such as those collected during the July 2010 cruise provide data critical for the validation and improvement of both particle trajectory and hydrodynamic models. Additionally the associated in situ surface measurements serve to verify altimetric current velocity fields and official surface oil forecast products. A combination of in situ hydrographic observations and remotely-sensed data demonstrate that the sequence of oceanographic events which occurred during the DWH oil spill (April–July 2010) ultimately resulted in the elimination of a direct circulation pathway between the northern GOM and the Straits of Florida. Thus the environmentally sensitive coastal habitats of south Florida and northern Cuba were spared the contamination experienced by northern Gulf coastal ecosystems. However, this may not necessarily be the case for future spills: the GOM circulation mode required for direct connectivity, wherein the LC is elongated into the northern GOM prior to LCR separation, occurs routinely and is well documented (and was the dominant

configuration in 2011; Lumpkin et al., 2011). In this scenario, downstream coastal regions in the GOM and Florida Straits are potential recipients of northern GOM waters and any associated contaminants. With direct pathway translation time-scales on the order of two to three weeks from the northern Gulf to the Florida Straits, an ocean observing system capable of sampling both the sea surface and the water column (through the use of multiple platforms) would benefit any long-term monitoring and impact mitigation efforts for the region.

## Acknowledgments

The authors gratefully acknowledge the officers and crew of the NOAA Ship *Nancy Foster* for their dedicated support in the field, the technicians and research assistants for their contributions both at sea and in the lab, the equipment and facilities of NOAA/AOML and NOAA/SEFSC, and the Response and Chemical Assessment Team (RCAT) laboratory at Louisiana State University for the hydrocarbon analysis. Special thanks are due to the NOAA leadership including Steve Murawski, Mike Uhart, Mike Allen, Craig McLean, and Judy Gray for facilitating the fieldwork at very short notice. The authors would also like to thank Christopher Meinen, Sang-Ki Lee, and Claudia Schmid for several helpful suggestions for improving earlier drafts of this manuscript. In addition to the laboratories listed above, financial support for this work was provided through NOAA Deepwater Horizon Supplemental Funding. NOAA Global Drifter Program drifter trajectory data referenced in this paper are available publicly at http://www.aoml.noaa.gov/envids/gld/dirkrig/parttrk_spatial_temporal.php).

## Appendix. SADCP and LADCP processing and section transports

Data collected from the shipboard Teledyne RD Instruments 150 kHz ADCP (SADCP) and the dual lowered Teledyne RD Instruments 300 kHz ADCPs (LADCPs) were used to observe the circulation features encountered across the survey domain. These data provided insight into the surface and subsurface spatial structure and temporal variability of the GOM circulation. They also allowed for the calculation of volume transports across the sections and features surveyed.

SADCP data were acquired with Teledyne RD Instruments *VMDas* software, which incorporated heading information from an Applanix *POS MV* directional GPS. Single ping SADCP data, originally binned at 4 m or 8 m (depending on the section), were processed utilizing CODAS, which yielded a data set of temporally averaged (5-min) profiles for the survey (http://currents.soest.hawaii.edu/docs/adcp_doc/codas_doc/). The maximum depth of the SADCP velocity profiles ranged from 200 to 350 m depending on bin size and ocean conditions.

Data collected by the paired LADCPs were logged internally during each CTD cast. Following the completion of each station, the data were uploaded and then processed using version 10.8 of the GEOMAR Visbeck software (Visbeck, 2002). This software incorporated external GPS, CTD, and SADCP data in the final velocity calculations for improved accuracy. The final velocity profile for each LADCP cast was binned to 10 m depth intervals. The maximum depth of each LADCP velocity profile was dependent upon the maximum depth of the corresponding CTD cast. Over the course of the survey, CTD casts were conducted from the surface to the bottom, or to 2000 m, whichever was shallower.

Mean velocity errors of the final processed SADCP and LADCP velocity profiles were estimated to be less than 5 cm $s^{-1}$. Velocity section plots were produced by linearly interpolating these two data sets onto a 10 m (vertical) by 1000 m (horizontal) resolution grid. A normal velocity grid was then generated based upon the section orientation, in order to quantify the perpendicular flow passing across the section (e.g. Fig. 5b, 5d, 5f, and 5h). The volume transports associated with these sections and the cross-sectional area limits/boundaries utilized in determining these flow rates are described below:

### *Section A (Florida Straits)*

The volume transport associated with the flow recorded along Section A (Figs. 4 and 6) between Key West and Havana, was found to be 29.6 Sv, with a maximum surface velocity of 172 cm $s^{-1}$. This volume transport agrees well with the highly-resolved transport time-series at 27°N in the Florida Straits (mean volume transport = 32.1 Sv; Meinen et al., 2010) and previous estimates of flow through Old Bahama and Northwest Providence Channels (Johns et al., 2002). The cross-sectional area used in this calculation was determined by the section bathymetry across the Florida Straits at this location. Velocity data were linearly extrapolated to this boundary. Due to the fact that no data were collected within the territorial waters of Cuba (12 NM), the extrapolated area accounted for 17% of the total cross-sectional area and approximately 1.4 Sv of the calculated total volume transport.

### *Section G (cyclonic eddy)*

The radial transport of the upper 1000 m of the cyclonic eddy that aided in the separation of EF from the LC (bisected by Section G in Figs. 4 and 6), was calculated to be 42.9 Sv. The cross-sectional area for this calculation was determined by flow characteristics along the northern eddy radius measured during Section G (velocity cross section not shown). Grid cells outside the zero velocity contour, south of the center of circulation and north of the cyclonic flow, were excluded. Grid cells located below 1000 m depth were also excluded.

### *Section L and Section M (EF)*

During the survey, two radial sections were occupied across EF: Section L and Section M (Fig. 5e–h). Based upon the anticyclonic EF flow structure observed along section M, the associated eddy circulation was determined to extend to approximately 1120 m depth. For comparison, radial transport calculations for both sections were limited to this depth (i.e. grid cells deeper than 1120 m were excluded). For Section L, grid cells outside the zero velocity contour, west of the center of circulation and east of the anticyclonic flow, were also excluded. Along section M, grid cells outside the zero velocity contour associated with the eastward anticyclonic flow (which extended to a depth of 1120 m) were excluded. As previously mentioned, the subsurface velocity structure and CTD $\theta$–$S$ profiles were examined to determine the approximate radius of EF along Section M. Grid cells north of this distance (175 km) were also excluded from the transport calculation.

Based on these two sections, EF radial transport (from the surface to 1120 m) was calculated to be between 38.2 and 43.6 Sv (Sections M and L respectively). One should note that with only three lowered velocity profiles obtained from within EF along Section M (due to limited ship time), unresolved finer-scale velocity structure at depths greater than 250 m may have contributed to error in the 38.2 Sv Section M radial transport.

## Reference


Adcroft, A., Hallberg, R., Dunne, J.P., Samuels, B.L., Galt, J.A., Barker, C.H., Payton, D., 2010. Simulations of underwater plumes of dissolved oil in the Gulf of Mexico. Geophys. Res. Lett. 37 (L18605), http://dx.doi.org/10.1029/2010GL044689.

Bugden, J.B.C., Yeung, C.W., Kepkay, P.E., Lee, K., 2008. Application of ultraviolet fluorometry and excitation-emission matrix spectroscopy (EEMS) to fingerprint oil and chemically dispersed oil in seawater. Mar. Pollut. Bull. 56, http://dx.doi.org/10.1016/j.marpolbul.2007.12.022. (677-585).

Camilli, R., Reddy, C.M., Yoerger, D.R., Van Mooy, B.A., Jakuba, M.V., Kinsey, J.C., McIntyre, C.P., Sylva, S.P., Maloney, J.V., 2010. Tracking hydrocarbon plume transport and biodegradation at Deepwater Horizon. Science 330, 201–204, http://dx.doi.org/10.1126/science.1195223.

DeHaan, C.J., Sturges, W., 2005. Deep cyclonic circulation in the Gulf of Mexico. J. Phys. Oceanogr. 35, 1801–1812, http://dx.doi.org/10.1175/JPO2790.1.

Diercks, A-R., Highsmith, R.C., Asper, V.L., Joung, D., Zhou, Z., Guo, L., Shiller, A.M., Joye, S.B., Teske, A.P., Guinsso, N., Wade, T.L., Lohrenz, S.E., 2010. Characterization of subsurface polycyclic aromatic hydrocarbons at the Deepwater Horizon site. Geophys. Res. Lett. 37, L20602, http://dx.doi.org/10.1029/2010GL045046.

Elliot, B.A., 1982. Anticyclonic rings in the Gulf of Mexico. J. Phys. Oceanogr. 12, 1292–1309, http://dx.doi.org/10.1175/1520-0485(1982)012<1292:ARITGO>2.0.CO;2.

Goni, G.J., Trinanes, J.A., MacFadyen, A., Streett, D., Olascoaga, M.J., Imhoff, M.L., Muller-Karger, F., Roffer, M.A., 2013. Variability of the Deepwater Horizon surface oil spill extent and its relationship to varying ocean currents and extreme weather conditions. Int. J. Remote Sens. (submitted for publication).

Green, D., B. Humphrey, B. Fowler, 1983. The use of flow-through fluorometry for tracking dispersed oil. In: Proceeding of the 1983 Oil Spill Conference, American Petroleum Institute Publication No. 4356, Washington D.C., pp. 473–475.

Hamilton, P., 2009. Topographic Rossby waves in the Gulf of Mexico. Prog. Oceanogr. 82, 1–31, http://dx.doi.org/10.1016/j.pocean.2009.04.019.

Hamilton, P., 1990. Deep currents in the Gulf of Mexico. J. Phys. Oceanogr. 20, 1087–1104, http://dx.doi.org/10.1175/1520-0485(1990)020<1087:DCITGO>2.0.CO;2.

Hazen, T.C., Dubinsky, E.A., DeSantis, T.Z., Andersen, G.L., Piceno, Y.M., Singh, N., Jansson, J.K., Probst, A., Borglin, S.E., Fortney, J.L., Stringfellow, W.T., Bill, M., Conrad, M.E., Tom, L.M., Chavarria, K.L., Alusi, T.R., Lamendella, R., Joyner, D.C., Spier, C., Baelum, J., Auer, M., Zemla, M.L., Chakraborty, R., Sonnenthal, E.L., D'Haseseleer, P., H-Y., Holman, N., Osman, S., Lu, Z., Van Nostrand, J.D., Deng, Y., Zhou, J., Mason, O.U., 2010. Deep-sea oil plume enriches indigenous oil-degrading bacteria. Science 330, 204–208, http://dx.doi.org/10.1126/science.1195979.

Henry, C.B., P.O. Roberts, E.B. Overton, 1999. A primer on in situ fluorometry to monitor dispersed oil. In: Proceeding of the 1999 International Oil Spill Conference, American Petroleum Institute Publication No. 4686b, Washington D.C., pp. 225–228.

Hetland, R.D., Hsueh, Y., Leben, R.R., Niiler, P.P., 1999. A loop-current-induced jet along the edge of the West Florida Shelf. Geophys. Res. Lett. 26 (15), 2239–2242, http://dx.doi.org/10.1029/1999GL900463.

Hu, C., Nelson, J.R., Johns, E., Chen, Z., Weisberg, R.H., Muller-Karger, F.E., 2005. Mississippi River water in the Florida Straits and in the Gulf Stream off Georgia in summer 2004. Geophys. Res. Lett. 32 (L14606), http://dx.doi.org/10.1029/2005GL022942.

Jochens, A.E., DiMarco, S.F., 2008. Physical oceanographic conditions in the Deepwater Gulf of Mexico in summer 2000–2002. Deep Sea Res. Part II 55, 2541–2554, http://dx.doi.org/10.1016/j.dsr2.2008.07.003.

Johns, W.E., Townsend, T.L., Fratantoni, D.M., Wilson, W.D., 2002. On the Atlantic inflow to the Caribbean Sea. Deep Sea Res. Part I 49, 211–243, http://dx.doi.org/10.1016/S0967-0637(01)00041-3.

Joye, S.B., MacDonald, I.R., Leifer, I., Asper, V., 2011. Magnitude and oxidation potential of hydrocarbon gases released from the BP oil well blowout. Nat. Geosci. 4, 160–164, http://dx.doi.org/10.1038/ngeo1067.

Kaiser, M.J., Pulsipher, A.G., 2007. The impact of weather and ocean forecasting on hydrocarbon production and pollution management in the Gulf of Mexico. Energy Policy 35, 966–983.

Kessler, J.D., Valentine, D.L., Redmond, M.C., Du, M., Chan, E.W., Mendes, S.D., Quiroz, E.W., Villanueva, C.J., Shusta, S.S., Werra, L.M., Yvon-Lewis, S.A., Weber, T.C., 2011. A persistent oxygen anomaly reveals the fate of spilled methane in the deep Gulf of Mexico. Science 331, 312–315, http://dx.doi.org/10.1126/science.1199697.

Liu, Y., Weisberg, R.H., Hu, C., Kovach, C., Riethmüller, R., 2011a. Evolution of the Loop Current system during the Deepwater Horizon oil spill event as observed with drifters and satellites. In: Liu, Y., et al. (Eds.), Monitoring and Modeling the Deepwater Horizon Oil Spill: A Record-Breaking Enterprise. Geophysical Monograph Series, vol. 195. AGU, Washington, D.C., pp. 91–101, http://dx.doi.org/10.1029/2011GM001127.

Liu, Y., Weisberg, R.H., Hu, C., Kovach, C., Zheng, L., 2011b. Trajectory forecast as a rapid response to the Deepwater Horizon oil spill. In: Liu, Y., et al. (Eds.), Monitoring and Modeling the Deepwater Horizon Oil Spill: A Record-Breaking Enterprise, Geophysical Monograph Series, vol. 195. AGU, Washington, D.C., pp. 153–165, http://dx.doi.org/10.1029/2011GM001121.

Lubchenco, J., M.K. McNutt, G. Dreyfus, S.A. Murawski, D.M. Kennedy, P.T. Anastas, S. Chu, T. Hunter, 2012. Science in support of Deepwater Horizon response. In: Proceedings of the National Academy of Sciences USA 109(50), 20212-20221, http://dx.doi.org/10.1073/pnas.1204729109.

Lumpkin, R., Grodsky, S., Centurioni, L., Rio, M., Carton, J., Lee, D., 2013. Removing spurious low-frequency variability in drifter velocities. J. Atmos. Oceanic Technol. 30, 353–360, http://dx.doi.org/10.1175/JTECH-D-12-00139.1.

Lumpkin, R., Goni, G., Dohan, K., 2011. State of the Ocean in 2010: Surface Currents. In: Blunden, J., Arndt, D.S., Baringer, M.O. (Eds.), State of the Climate in 2010, 92. Bulletin of American Meteorological Society, pp. S92–S95.

MacFadyen, A., Watabayashi, G.Y., Barker, C.H., Beegle-Krause, C.J., 2011. Tactical modeling of surface oil transport during the Deepwater Horizon spill response. In: Liu, Y., et al. (Eds.), Monitoring and Modeling the Deepwater Horizon Oil Spill: A Record-Breaking Enterprise, Geophysical Monograph Series, vol. 195. AGU, Washington, D.C., pp. 167–178, http://dx.doi.org/10.1029/2011GM001128.

Meinen, C.S., Baringer, M.O., Garcia, R.F., 2010. Florida Current transport variability: an analysis of annual and longer-period signals. Deep Sea Res. Part I 57, 835–846, http://dx.doi.org/10.1016/j.dsr.2010.04.001.

National Oceanic and Atmospheric Administration, 2012. Natural Resource Damage Assessment April 2012 Status Update for the Deepwater Horizon Oil Spill, pp. 74–75. ⟨http://www.gulfspillrestoration.noaa.gov/wp-content/uploads/FINAL_NRDA_StatusUpdate_April2012.pdf⟩.

Niiler, P.P., Sybrandy, A., Bi, K., Poulain, P., Bitterman, D., 1995. Measurements of the water-following capability of holey-sock and TRISTAR drifters. Deep Sea Res. Part I 42, 1951–1964, http://dx.doi.org/10.1016/0967-0637(95)00076-3.

Nowlin Jr., W.D., 1972. Winter circulation patterns and property distributions. In: Capurro, L.R.A., Reid, J.L. (Eds.), Contributions on the Physical Oceanography of the Gulf of Mexico. Gulf Publishing, pp. 3–52.

Nowlin Jr., W.D., McLellan, H.J., 1967. A characterization of the Gulf of Mexico waters in winter. J. Mar. Res. 25, 29–59.

Oey, L., Lee, H.C., 2002. Deep eddy energy and topographic Rossby waves in the Gulf of Mexico. J. Phys. Oceanogr. 32, 3499–3527, http://dx.doi.org/10.1175/1520-0485(2002)032<3499:DEEATR>2.0.CO;2.

Oey, L.Y., Ezer, T., Lee, H.C., 2005. Loop Current, rings, and related circulation in the Gulf of Mexico: a review of numerical models and future challenges. In: Sturges, W., Lugo-Fernandez, A. (Eds.), Circulation in the Gulf of Mexico: Observations and Models. Geophysical Monograph Series, vol. 161. AGU, Washington, D.C., pp. 31–56, http://dx.doi.org/10.1029/161GM04.

Ortner, P.B., Lee, T.N., Milne, P.J., Zika, R.G., Clarke, M.E., Podesta, G.P., Swart, P.K., Tester, P.A., Atkinson, L.P., Johnson, W.R., 1995. Mississippi River flood waters that reached the Gulf Stream. J. Geophys. Res. 100 (C7), 13595–13601, http://dx.doi.org/10.1029/95JC01039.

Olascoaga, M.J., Rypina, I.I., Brown, M.G., Beron-Vera, F.J., Koçak, H., Brand, L.E., Halliwell, G.R., Shay, L.K., 2006. Persistent transport barrier on the West Florida Shelf. Geophys. Res. Lett. 33 (L22603), http://dx.doi.org/10.1029/2006GL027800.

Paluszkiewicz, T., Atkinson, L.P., Posmentier, E.S., McClain, C.R., 1983. Observations of a Loop Current frontal eddy intrusion onto the west Florida shelf. J. Geophys. Res. 88 (C14), 9639–9651, http://dx.doi.org/10.1029/JC088iC14p09639.

Parsons, A.R., Cross, S.L., 2010. A collaborative report on the synthesis of subsurface data from the Deepwater Horizon response effort. Abstract OS21G-04 presented at 2010 Fall Meeting, AGU, San Francisco, California, 13–17 Dec.

Ramseur, J.L., Hagerty, C.L., 2013. Deepwater Horizon Oil Spill: Recent Activities and Ongoing Developments. 31 January 2013. R42942 FAS CRS Reports. Web. 1 July 2013.

Rio, M.H., Guinehut, S., Larnicol, G., 2011. New CNES-CLS09 global mean dynamic topography computed from the combination of GRACE data, altimetry, and in situ measurements. J. Geophys. Res. 116 (C07018), http://dx.doi.org/10.1029/2010JC006505.

Ryan, J.P., Zhang, Y., Thomas, H., Rienecker, E.V., Nelson, R.K., Cummings, S.R., 2011. A high-resolution survey of a deep hydrocarbon plume in the Gulf of Mexico during the 2010 Macondo blowout. In: Liu, Y., et al. (Eds.), Monitoring and Modeling the Deepwater Horizon Oil Spill: A Record-Breaking Enterprise, Geophysical Monograph Series, vol. 195. AGU, Washington, D.C., pp. 63–75, http://dx.doi.org/10.1029/2011GM001106.

Schmitz, W.J., Biggs, D.C., Lugo-Fernandez, A., Oey, L.-Y., Sturges, W., 2005. A synopsis of the circulation in the Gulf of Mexico and on its continental margins. In: Sturges, W., Lugo-Fernandez, A. (Eds.), Circulation in the Gulf of Mexico: Observations and Models, Geophysical Monograph Series, vol. 161. AGU, Washington, D.C., pp. 11–29, http://dx.doi.org/10.1029/161GM03.

Schroeder, W.W., Berner Jr., L., Nowlin Jr., W.D., 1974. The oceanic waters of the Gulf of Mexico and Yucatan Strait during July 1969. Bull. Mar. Sci. 24 (1), 1–19.

Shay, L.K., Jaimes, B., Brewster, J.K., Meyers, P., McCaskill, E.C., Uhlhorn, E., Marks, F., Halliwell Jr., G.R., Smedstad, O.M., Hogan, P., 2011. Airborne ocean surveys of the Loop Current complex from NOAA WP-3D in support of the Deepwater Horizon oil spill. In: Liu, Y., et al. (Eds.), Monitoring and Modeling the Deepwater Horizon Oil Spill: A Record-Breaking Enterprise, Geophysical Monograph Series, vol. 195. AGU, Washington, D.C., pp. 131–151, http://dx.doi.org/10.1029/2011GM001101.

Smith, R.H., G.J. Goni, E.M. Johns, A.M. Wood, 2010. NF1013 Mission Summary Report, ⟨http://www.noaa.gov/sciencemissions/PDFs/NF1013_mission_summary_report.pdf⟩.

Streett, D., 2011. NOAA's satellite monitoring of marine oil. In: Liu, Y., et al. (Eds.), Monitoring and modeling the Deepwater Horizon Oil Spill: A Record-Breaking Enterprise, Geophysical Monograph Series, vol. 195. AGU, Washington, D.C., pp. 9–18, http://dx.doi.org/10.1029/2011GM001104.

Sturges, W., Leben, R., 2000. Frequency of ring separations from the Loop Current in the Gulf of Mexico: a revised estimate. J. Phys. Oceanogr. 30, 1814–1819, http://dx.doi.org/10.1175/1520-0485(2000)030<1814:forsft>2.0.co;2.

Valentine, D.L., Kessler, J.D., Redmond, M.C., Mendes, S.D., Heintz, M.B., Farwell, C., Hu, L., Kinnaman, F.S., Yvon-Lewis, S., Du, M., Chan, E.W., Tigreros, F.G.,

Villanueva, J., 2010. Propane respiration jump-starts microbial response to a deep oil spill. Science 330, 208–211, http://dx.doi.org/10.1126/science.1196830.
Visbeck, M., 2002. Deep velocity profiling using lowered acoustic Doppler current profilers: bottom track and inverse solutions. J. Atmos. Oceanic Technol. 19, 794–807, http://dx.doi.org/10.1175/1520-0426(2002)019<0794:DVPULA>2.0.CO;2.
Vukovich, F.M., Maul, G.A., 1985. Cyclonic eddies in the eastern Gulf of Mexico. J. Phys. Oceanogr. 15, 105–117, http://dx.doi.org/10.1175/1520-0485(1985)015<0105:CEITEG>2.0.CO;2.
Wade, T.L., Sweet, S.T., Walpert, J.N., Sericano, J.L., Singer, J.J., Guinasso Jr., N.L., 2011. Evaluation of possible inputs of oil from the Deepwater Horizon spill to the Loop Current and associated eddies in the Gulf of Mexico. In: Liu, Y., et al. (Eds.), Monitoring and Modeling the Deepwater Horizon Oil Spill: A Record-Breaking Enterprise, Geophysical Monograph Series, vol. 195. AGU, Washington, D.C., pp. 83–90, http://dx.doi.org/10.1029/2011GM001095.
Wells, Kent, 2010. Kent Wells BP Technical Briefing July 15, 2010 2:30 p.m. CT (transcript), ⟨http://www.bp.com/liveassets/bp_internet/globalbp/globalbp_uk_english/gom_response/STAGING/local_assets/downloads_pdfs/kent_wells_technical_briefing_transcript_15_07_1430CDT.pdf⟩.
Wood, A.M., 2010. WS1010A Mission Summary Report, ⟨http://www.noaa.gov/deepwaterhorizon/publications_factsheets/documents/mission_summary/WaltonSmithMissionReport_June_6-10_2010_Mission.pdf⟩.
Yang, H., Weisberg, R.H., Niiler, P.P., Sturges, W., Johnson, W., 1999. Lagrangian circulation and forbidden zone on the West Florida Shelf. Cont. Shelf Res. 19, 1221–1245, http://dx.doi.org/10.1016/S0278-4343(99)00021-7.
Zavala-Hidalgo, J., Morey, S.L., O'Brien, J., 2003. Cyclonic eddies northeast of the Campeche Bank from altimetry data. J. Phys. Oceanogr. 23, 623–629, http://dx.doi.org/10.1175/1520-0485(2003)033<0623:CENOTC>2.0.CO;2.